This article may be downloaded for personal use only. Any other use requires prior permission of the author and AIP Publishing. This article appeared in Appl. Phys. Lett. 111, 253103 (2017) and may be found at https://doi.org/10.1063/1.4997774.

APPLIED PHYSICS LETTERS **111**, 253103 (2017)

Chemical vapour deposition of freestanding sub-60 nm graphene gyroids

Tomasz Cebo,[1] Adrianus I. Aria,[1,2] James A. Dolan,[1,3,4] Robert S. Weatherup,[1,5] Kenichi Nakanishi,[1] Piran R. Kidambi,[6] Giorgio Divitini,[7] Caterina Ducati,[7] Ullrich Steiner,[4] and Stephan Hofmann[1,a)]

[1]*Department of Engineering, University of Cambridge, Cambridge CB3 0FA, United Kingdom*
[2]*Surface Engineering and Nanotechnology Institute, Cranfield University, Cranfield MK43 0AL, United Kingdom*
[3]*Department of Physics, University of Cambridge, Cambridge CB3 0HE, United Kingdom*
[4]*Adolphe Merkle Institute, University of Fribourg, Fribourg CH-1700, Switzerland*
[5]*Department of Chemistry, University of Cambridge, Cambridge, CB2 1EW, United Kingdom*
[6]*Department of Chemical and Biomolecular Engineering, Vanderbilt University School of Engineering, 2301 Vanderbilt Place PMB 351826, Nashville, Tennessee 37235-1826, USA*
[7]*Department of Materials Science and Metallurgy, University of Cambridge, Cambridge CB3 0FS, United Kingdom*

(Received 26 July 2017; accepted 21 November 2017; published online 18 December 2017)

The direct chemical vapour deposition of freestanding graphene gyroids with controlled sub-60 nm unit cell sizes is demonstrated. Three-dimensional (3D) nickel templates were fabricated through electrodeposition into a selectively voided triblock terpolymer. The high temperature instability of sub-micron unit cell structures was effectively addressed through the early introduction of the carbon precursor, which stabilizes the metallized gyroidal templates. The as-grown graphene gyroids are self-supporting and can be transferred onto a variety of substrates. Furthermore, they represent the smallest free standing periodic graphene 3D structures yet produced with a pore size of tens of nm, as analysed by electron microscopy and optical spectroscopy. We discuss generality of our methodology for the synthesis of other types of nanoscale, 3D graphene assemblies, and the transferability of this approach to other 2D materials. *Published by AIP Publishing.*
https://doi.org/10.1063/1.4997774

2D materials not only offer unique functionality as planar atomically thin layers but can also be engineered into complex 3D structures, allowing the design of a new class of materials with tailored mechanical, thermal, electrical, and optical properties, ultra-low densities, and high surface areas. The recent literature highlights the promise of such porous, foam-like materials, in particular those derived from graphene, in applications ranging from (opto)electronics,[1,2] artificial skin,[3] electrochemistry,[4–6] and catalysis[7] to thermal management,[8] self-cleaning,[9] sorption and filtration,[10] sensors,[11] bio-medical,[12] and mechanical metamaterials.[13,14] Among the various synthetic strategies and 3D assembly approaches,[15] chemical vapour deposition (CVD) has emerged as the most viable route not only to grow highly crystalline 2D material films but also to directly grow covalently bonded, continuous 3D networks of these 2D materials.[1,16,17] For the latter, the CVD approach essentially relies on a 3D template that can be exposed to growth conditions at high enough temperatures to crystallise 2D materials on its surface. Transition metal templates are particularly promising, with catalytic properties that enable the synthesis of highly crystalline graphene at relatively low temperatures.[17,18] While numerous methods to create suitable 3D metal templates have been demonstrated, ranging from commercial metal foams[1] and the sintering of metal powders[4,5] to 3D printing[19] and two-photon lithography,[20] the bottleneck remains 3D template control and accessible sizes/resolution. Typical metal foams have pore diameters of the order of 100 μm,[1] and over such large length-scales 3D structures based on mono- or few-(<20) layer graphene are not sufficiently mechanically stable, i.e., when the metal template is etched away, they are prone to collapse. The smallest pore sizes demonstrated to date are of the order of 1 μm.[4,20] More recently, nano-porous zeolites decorated with Lanthanum have been used as a template to create carbon frameworks, albeit not fully graphitised.[7] Furthermore, computational modelling has recently highlighted the potentially exceptional properties of periodic gyroid graphene structures.[13] A well-known challenge, in particular for pure metal templates, is their high self-diffusivity,[21] which means that metal templates with sub-100 nm unit cell sizes are prone to sintering, i.e., they are not stable at the required elevated CVD temperatures.

Here, we demonstrate the direct CVD of freestanding graphene gyroids with controlled sub-60 nm unit cell sizes. We use Ni gyroidal templates prepared through electrodeposition into a selectively voided triblock terpolymer.[22] The high temperature instabilities of sub-micron unit cell structures are avoided through the early introduction of the carbon precursor, which is found to stabilize the metallized gyroidal templates.[23] The as-grown graphene gyroids are self-supporting with less than 15 layers of graphitic wall thickness and can be transferred from the deposition substrate. We analyse their structure by electron microscopy and optical spectroscopy. We discuss the generality of our methodology for the synthesis of other types of freestanding 2D material assemblies on the sub-micron scale.

Figure 1 schematically highlights the synthesis process used to form freestanding graphene gyroids (see Methods in the supplementary material for more details). The initial polymer templates were fabricated through the self-assembly of polyisoprene-block-polystyrene-block-poly(ethylene oxide) (ISO) triblock copolymer [Fig. 1(a)], consisting of linearly

a)Author to whom correspondence should be addressed: sh315@cam.ac.uk

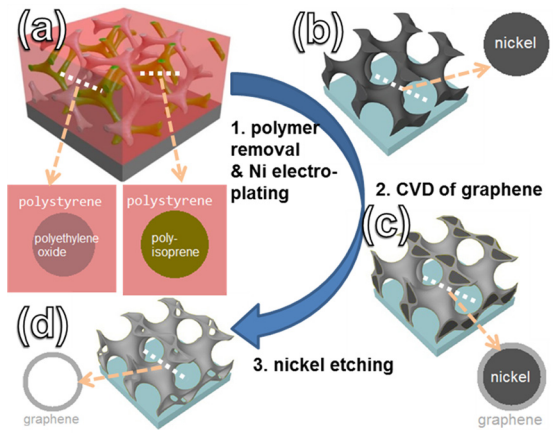

FIG. 1. (a) Schematic geometry and composition of the alternating gyroid (gyroidal) phase of the ISO triblock copolymer: red, polystyrene matrix; blue, polyethylene oxide gyroid network; and green, polyisoprene gyroid network. (b) Nickel gyroid prepared by electroplating into the empty space left after polyisoprene removal. (c) Nickel gyroid covered in graphene after CVD with the acetylene precursor. (d) Self-standing graphene gyroid after nickel removal with ferric chloride solution. The insets show cross-sections of the respective gyroid along the indicated white lines.

connected polyisoprene (PI), poly(ethylene oxide) (PEO), and polystyrene (PS) blocks.[22] ISO of different molecular weights was used to obtain polymer templates with different unit cell sizes. Polymer gyroids with unit cell sizes of ∼35 nm and ∼60 nm were fabricated using ISO of ∼33 kg/mol and ∼80 kg/mol, respectively.[24] They were deposited on conductive fluorine-doped tin oxide (FTO)-coated glass and thermally annealed in a vacuum oven to form the desired microphase-separated morphology. PI was subsequently removed from the ISO polymer templates by UV exposure and an ethanol rinse. These polymer templates were then metallized by electroplating Ni into the voids left after PI removal, using the FTO-coated glass as a working electrode. The remaining polymers were subsequently removed by oxygen plasma etching. Polymer removal resulted in gyroidal Ni templates (denoted further as G35_Ni for 35 nm unit cell size and G60_Ni for 60 nm unit cell size) that structurally resemble the original polymer templates [Fig. 1(b)].[25] Graphene layers were then catalytically grown on the Ni surface by CVD [Fig. 1(c)]. CVD was performed using pure acetylene (C_2H_2) as the precursor at 2.2×10^{-3} mbar and heating to 550–650 °C, as discussed below. The resulting structures are denoted as G60_Ni+G and G35_Ni+G. After CVD, Ni was removed by etching with an aqueous $FeCl_3$ solution, resulting in freestanding graphene gyroids. Consequently, these are denoted as G60_G and G35_G. These graphene gyroids can then be easily transferred by etching away the underlying FTO layer with HCl followed by a lift-off process and transfer onto a glass slide for rinsing in deionised water (DI) water and then eventually onto the desired substrate. As shown below, the as-fabricated graphene gyroids are freestanding and are stable enough to support their own weight. Hence, the transfer can be achieved without additional polymer support, unlike in the standard graphene poly(methyl methacrylate) (PMMA) transfer [see Fig. S.I(a) in the supplementary material].[26,27]

Figure 2 shows SEM analysis of the gyroid structure at the various process stages. CVD allows the fabrication of freestanding graphene gyroids across large areas. As shown in Fig. S.I(b) (supplementary material), graphene gyroids can already be fabricated over cm^2 areas. Optically, freestanding graphene gyroids are similar in appearance to the nickel templates although they appear more transparent [Figs. S.II(a)–S.II(d), supplementary material]. SEM images show that both G60_G and G35_G have inherited the shape and scale of their respective nickel templates—G60_Ni and G35_Ni, with unit cells of ∼60 nm and ∼35 nm (Figs. 2(a)–2(f), respectively). Energy dispersive X-ray spectroscopy (EDX) [Fig. S.II(e), supplementary material] show no Ni peak, consistent with the removal of Ni. The O, Si, and Sn peaks in the graphene gyroid EDX spectrum originate from the underlying FTO glass and are more prominent than for the nickel gyroids due to the higher electron and x-ray transparency of the graphene gyroids.[28,29] Nickel X-ray excitation energies are $K\alpha = 7.480$ keV and $L\alpha = 0.849$ keV. With 12 kV acceleration energy, the $L\alpha$ peak is prominent and the $K\alpha$ peak is weak. These peaks are not observed at all in the EDX spectra of the graphene gyroids. The graphene gyroids display good electrical properties—∼500 nm thick G60_G transferred on non-conductive glass exhibited a sheet resistance of 240 Ω/sq (see supplementary material for details).

The Raman spectra in Fig. 3(a) compare G60_G deposited with a maximum process temperature of 650 °C, with graphene deposited under similar conditions on Ni foam (∼100 μm pore size),[1] Ni foil (25 μm thick) and Ni film (500 nm thick), with the major difference being the heat conductivities and thicknesses of the substrates. G60_G is also compared with G35_G deposited with a lower maximum process temperature (550 °C). The Raman spectra of

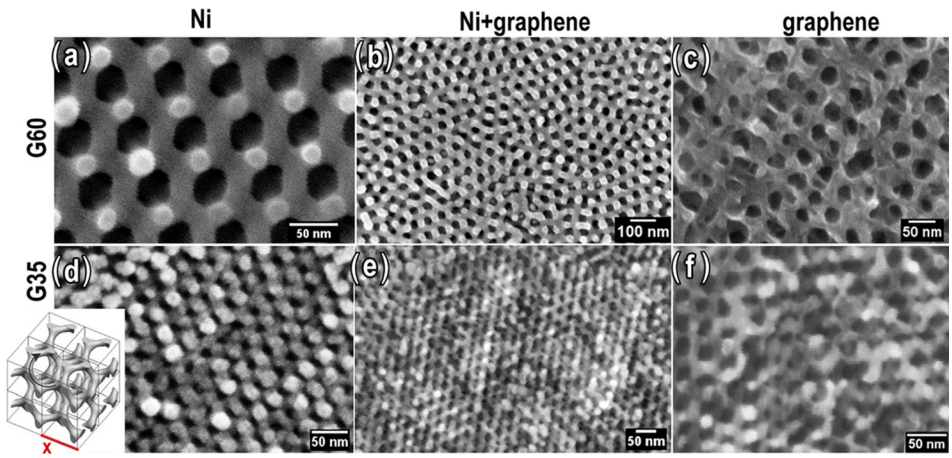

FIG. 2. Gyroids of two unit cell sizes: 60 nm (G60) and 35 nm (G35) analysed by SEM: (a) G60_Ni nickel template. (b) G60_Ni+G nickel template with graphene—after CVD. (c) Free standing graphene G60_G—after nickel etching. (d). G35_Ni nickel template. (e) G35_Ni+G nickel template with graphene—after CVD. (f) Free standing graphene G35_G—after nickel etching. The inset schematically highlights eight unit cells of the gyroid structure, where x is 60 nm for G60 and 35 nm for G35.

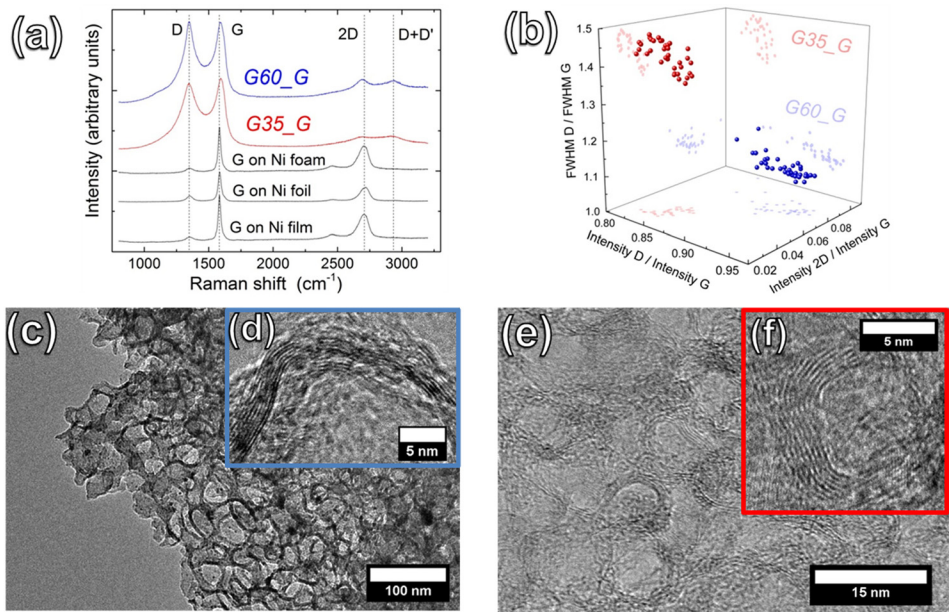

FIG. 3. (a) Raman spectra of graphene on a 500 nm thick Ni film (bottom black line), graphene on 25 μm thick Ni foil (middle black line), graphene on Ni foam (top black line), G35_G (red line), and G60_G (blue line). (b) 3D plot of the D/G ratio versus 2D/G peak intensities versus the ratio of the full width at half maximum of the D/G Raman peaks; G35_G (red) and G60_G (blue). The shaded spots are projections of data onto the three planes. Each group of points contains 36 measurements spanning 25 × 25 μm areas. [(c) and (e)] HRTEM images of G60_G and G35_G, respectively, with close-ups into single gyroid channels with diameters of (d) ~15 nm and (f) ~5 nm, respectively.

graphene deposited on 3D gyroidal structures differ significantly from those of the graphene deposited on flat substrates despite very similar growth conditions. The Raman spectra of the foam, foil, and film are characteristic of flat, few-layer graphene.[30] In contrast, the spectra of G60_G and G35_G display prominent and wide D and G peaks with an intensity ratio (I_D/I_G) of ~1. The prominence of the D peaks in both G60_G and G35_G is attributable to the presence of many small and disordered graphene domains.[31,32] The G band for the gyroids appears at a higher wavenumber than for the flat substrates, which is consistent with the presence of strained nanosized graphene layers.[33] Figure 3(b) presents a 3D plot of I_D/I_G vs. I_{2D}/I_G vs. $FWHM_D/FWHM_G$ (ratio of the full widths at half maximum of the peaks). The plot has two separated clusters of data points indicating a significant difference between G35_G and G60_G. We suggest that this results from the different radii of curvatures of the supports on which the graphene conformally grows. The lower I_{2D}/I_G for G35_G can be attributed to larger strain present in double C=C bonded chains due to the higher curvature.[34] Broadening of the D peak, shown by both higher $FWHM_D/FWHM_G$ and lower I_D/I_G for G35_G, could indicate higher disorder caused by smaller grain sizes and a higher density of non-six member rings required to conform to the high curvature.[35] This is also consistent with the fact that when G35_G is grown at lower temperatures, recrystallization, self-healing, and merging of domains could not happen to the same extent as in G60_G (discussed further below). Finally, it is prudent to mention that Ni used as a CVD template comes from an electroplating solution, which might contain trace amounts of levelling agents and other impurities. These, even though present in very small amounts, may affect the nucleation density. However, a more detailed analysis is beyond the scope of this paper.

Figures 3(c)–3(f) show TEM images of G60_G [Figs. 3(c) and 3(d)] and G35_G [Figs. 3(e) and 3(f)]. It is evident that the structures are graphitic with few-layered graphene forming the walls of the channels. The observed crystal quality is consistent with the Raman results discussed above. The radii of the G60_G and G35_G pores are ~15 nm and ~5 nm, respectively, with about 10 layers forming the walls [Figs. 3(d) and 3(f)]. Both results are consistent with the geometry of gyroids (Fig. 2 inset). The lattice spacing observed in the TEM images is about 0.335 nm which corresponds well to the interlayer spacing of graphite.[36]

Figure 4 demonstrates the main challenge of CVD when using a nanoscale metal template—the instability of the metal catalyst at high temperatures. Unlike Ni foam templates with unit cell sizes of the order of hundreds of microns,[1] the sub-micron unit cells of Ni gyroid templates transform into bulky clusters at temperatures >500 °C. The formation of clusters is driven by the thermodynamic tendency to minimise the surface area, enabled by the increase in Ni self-diffusion with temperature.[37] Using a typical one-step CVD process,[18] where the hydrocarbon precursor is introduced only once the growth temperature has been reached, both G35_Ni and G60_Ni do not preserve their original morphologies and transform into large clusters already during the heating ramp [Fig. 4(a)]. To overcome this limitation, we introduce the carbon precursor right from the beginning of the heating ramp (predosing), which helps to stabilize the nickel templates and prevents the formation of Ni clusters at the growth temperature [Fig. 4(b)]. The following mechanisms may play a role in stabilising the template: During the initial heating of the template, precursor dissociation begins well below the maximum process temperature, with the supplied C being readily absorbed by the Ni template, given the reasonably large solubility of C in Ni.[38] When the Ni surface becomes saturated, the additional hydrocarbon dissociation feeds graphene nucleation at the Ni surface.[39] The relatively small bulk of the gyroids compared to thicker catalyst foams, foils, and films means that this point is reached at a lower temperature. Consistent with the Raman results discussed above, a higher nucleation density is thus expected as a result of the lower C diffusivity at this low nucleation temperature,[18] as well as the higher template curvature and thus an abundance of low-coordination sites which serve as preferential graphene nucleation sites. This

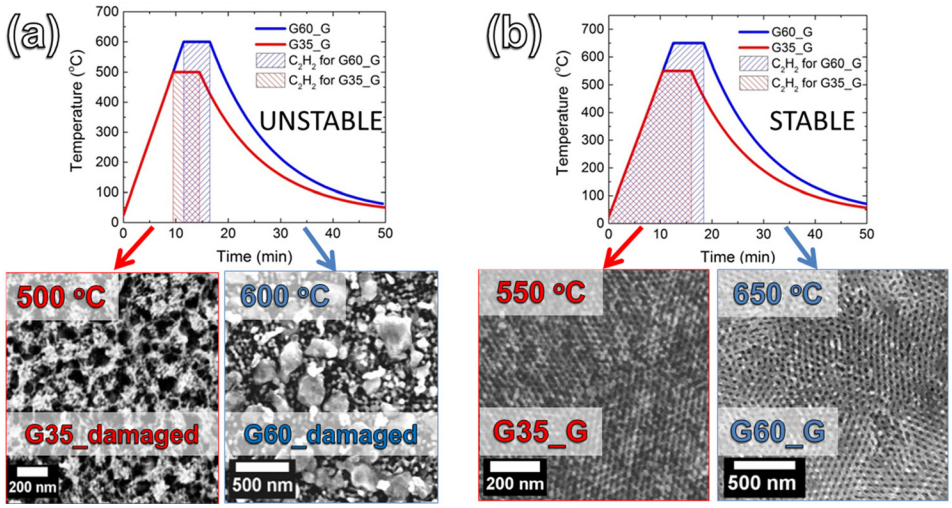

FIG. 4. Process diagrams presenting unstable (a) and stable (b) procedures for graphene gyroid preparation. The structures in (b) were stabilised by acetylene (gas precursor) preloading at RT. SEM images in (a) show damage to G35 and G60 at as low as 500 °C and 600 °C, respectively. SEM images in (b) show preserved G35_G and G60_G after processing at 550 °C and 650 °C, respectively. The process diagram in (b) also shows the optimal conditions for graphene gyroid preparation by CVD.

promotes the formation of small graphene islands of low graphitic quality which continue to grow isothermally as the precursor exposure continues to form a continuous graphitic network over the template.[40] These graphitic deposits are expected to exhibit a strong interaction with Ni, as a result of hybridisation between the graphene π and Ni 3d orbitals, thus helping to stabilise the template.[41] Additionally, nickel surface carbides are known to readily form at temperatures below 500 °C,[42] which may also assist in stabilising the template. As the process temperature continues to increase, amorphous and highly defective regions of the C coating are graphitised, which may involve defect healing and a re-dissolution process, as the C solubility in Ni increases with temperature. This ultimately yields the crystalline graphitic layers shown in the TEM images of Fig. 3.

Our approach can be extended both to other metal templates and to materials beyond graphene. The suitability of a given metal template will depend on its catalytic efficiency to induce graphitisation compared to its self-diffusivity at the given CVD temperature. Hence, the temperature instabilities of sub-micron unit cell structures can be similarly addressed for metals that in those respects show a similar behaviour to Ni,[37] such as Co,[43] or for metals, which require higher growth temperatures but have lower self-diffusivities, such as Pt.[44–46] For metals, such as Cu, which require higher temperatures for graphene growth and have high self-diffusivities (3 orders of magnitude higher for Cu than Ni at 900 °C),[47,48] successfully applying our approach may be more challenging. Nonetheless, there are further avenues to increase template stability, for instance, by plasma pre-coating. The challenge for 3D structural control is common to many different materials beyond graphene, including for instance ceramic foams. Ceramic foam structures, particularly those based on thermally and chemically stable boron nitride, have a wide application potential, ranging from mechanical metamaterials[49] to filtration and catalysis.[50] The templated CVD approach can be extended to fabricate free-standing hexagonal boron nitride (h-BN) gyroid structures. The template stabilisation for h-BN CVD is more complex to rationalise as the supply, solubility, and chemical behaviour of both B and N with respect to the catalyst template have to be considered. This connects to our previous detailed h-BN growth studies,[51,52] but an in-depth discussion of this goes beyond the scope of this paper. Similarly, without discussing the specific growth mechanisms involved, our approach can be extended to transition metal dichalcogenides, for instance, by using Au gyroids for WS_2 CVD.[53]

In summary, we demonstrate the controlled fabrication of graphene gyroids with sub-60 nm pore-sizes, produced by an optimised CVD process using Ni templates which were generated by electrodeposition into a selectively voided triblock terpolymer. The resulting freestanding graphene gyroids of two unit cell sizes, 35 nm and 60 nm, faithfully replicate the original polymer structure and show reasonable graphitic crystal quality with wall thicknesses below 15 layers. The early introduction of the carbon precursor suppressed the high temperature instability of sub-micron network morphologies. This approach can be extended to other metal templates and to materials beyond graphene. For a given template, this approach relies on its catalytic efficiency being sufficient to induce 2D material growth at temperatures where self-diffusivity is low enough that the structure remains stable. The demonstrated control of such foam-like materials on the sub-micron scale offers new or enhanced functionalities for a wide range of emerging applications where light-weight, high surface area, and mechanical stability are desirable.

See supplementary material for a detailed description of materials and methods, and additional data on graphene gyroids and pyrolithic conversion of the polymer template.

We acknowledge funding from EPSRC (Grant No. EP/K016636/1, GRAPHTED) and ERC (Grant Nos. 279342, InsituNANO, and 259619, PHOTO EM), as well as Cambridge University NanoDTC (Grant No. EPSRC EP/G037221/1). R.S.W. acknowledges a Research Fellowship from St. John's College, Cambridge, and a EU Marie Skłodowska-Curie Individual Fellowship under Grant ARTIST (No. 656870). U.S. acknowledges funding from the Adolphe Merkle foundation. T.C. acknowledges funding from M.B. Grabowski Fund.

[1]Z. Chen, W. Ren, L. Gao, B. Liu, S. Pei, and H.-M. Cheng, Nat. Mater. **10**, 424 (2011).
[2]Y. Ito, Y. Tanabe, H. Qiu, K. Sugawara, S. Heguri, N. H. Tu, K. K. Huynh, T. Fujita, T. Takahashi, K. Tanigaki, and M. Chen, Angew. Chem. **53**, 4822 (2014).

[3]C. Hou, T. Huang, H. Wang, H. Yu, Q. Zhang, and Y. Li, Sci. Rep. **3**, 3138 (2013).
[4]S. Drieschner, M. Weber, J. Wohlketzetter, J. Vieten, E. Makrygiannis, B. M. Blaschke, V. Morandi, L. Colombo, F. Bonaccorso, and J. A. Garrido, 2D Mater. **3**, 45013 (2016).
[5]J. Sha, C. Gao, S. K. Lee, Y. Li, N. Zhao, and J. M. Tour, ACS Nano **10**, 1411 (2016).
[6]K. Xi, P. R. Kidambi, R. Chen, C. Gao, X. Peng, C. Ducati, S. Hofmann, and R. V. Kumar, Nanoscale **6**, 5746 (2014).
[7]K. Kim, T. Lee, Y. Kwon, Y. Seo, J. Song, J. K. Park, H. Lee, J. Y. Park, H. Ihee, S. J. Cho, and R. Ryoo, Nature **535**, 131 (2016).
[8]M. T. Pettes, H. Ji, R. S. Ruoff, and L. Shi, Nano Lett. **12**, 2959 (2012).
[9]E. Singh, Z. Chen, F. Houshmand, W. Ren, Y. Peles, H.-M. Cheng, and N. Koratkar, Small **9**, 2 (2013).
[10]H. Bi, X. Xie, K. Yin, Y. Zhou, S. Wan, L. He, F. Xu, F. Banhart, L. Sun, and R. S. Ruoff, Adv. Funct. Mater. **22**, 4421 (2012).
[11]J. Liu, X. Wang, T. Wang, D. Li, F. Xi, J. Wang, and E. Wang, ACS Appl. Mater. Interfaces **6**, 19997 (2014).
[12]A. E. Jakus, E. B. Secor, A. L. Rutz, S. W. Jordan, and M. C. Hersam, ACS Nano **9**, 4636 (2015).
[13]Z. Qin, G. S. Jung, M. J. Kang, and M. J. Buehler, Sci. Adv. **3**, e1601536 (2017).
[14]L. Qiu, J. Z. Liu, S. L. Y. Chang, Y. Wu, and D. Li, Nat. Commun. **3**, 1241 (2012).
[15]P. C. Sherrell and C. Mattevi, Mater. Today **19**, 428 (2016).
[16]M. Mecklenburg, A. Schuchardt, Y. K. Mishra, S. Kaps, R. Adelung, A. Lotnyk, L. Kienle, and K. Schulte, Adv. Mater. **24**, 3486 (2012).
[17]S. Hofmann, P. Braeuninger-Weimer, and R. S. Weatherup, J. Phys. Chem. Lett. **6**, 2714 (2015).
[18]R. S. Weatherup, B. C. Bayer, R. Blume, C. Ducati, C. Baehtz, R. Schl, and S. Hofmann, Nano Lett. **11**, 4154 (2011).
[19]Z. Yang, C. Yan, J. Liu, S. Chabi, Y. Xia, and Y. Zhu, RSC Adv. **5**, 29397 (2015).
[20]J. Bauer, A. Schroer, R. Schwaiger, and O. Kraft, Nat. Mater. **15**, 438 (2016).
[21]H. Mehrer, *Landolt-Börnstein: Diffusion in Solid Metals and Alloys* (Springer-Verlag Berlin Heidelberg, 1990).
[22]S. Vignolini, N. A. Yufa, P. S. Cunha, S. Guldin, I. Rushkin, M. Stefik, K. Hur, U. Wiesner, J. J. Baumberg, and U. Steiner, Adv. Mater. **24**, OP23 (2012).
[23]B. C. Bayer, D. A. Bosworth, F. B. Michaelis, R. Blume, G. Habler, R. Abart, R. S. Weatherup, P. R. Kidambi, J. J. Baumberg, A. Knop-Gericke, R. Schloegl, C. Baehtz, Z. H. Barber, J. C. Meyer, and S. Hofmann, J. Phys. Chem. C **120**, 22571 (2016).
[24]S. Salvatore, A. Demetriadou, S. Vignolini, S. S. Oh, S. Wuestner, N. A. Yufa, M. Stefik, U. Wiesner, J. J. Baumberg, O. Hess, and U. Steiner, Adv. Mater. **25**, 2713 (2013).
[25]J. A. Dolan, M. Saba, R. Dehmel, I. Gunkel, Y. Gu, U. Wiesner, O. Hess, T. D. Wilkinson, J. J. Baumberg, U. Steiner, and B. D. Wilts, ACS Photonics **3**, 1888 (2016).
[26]A. Reina, H. Son, L. Jiao, B. Fan, M. S. Dresselhaus, Z. Liu, and J. Kong, Phys. Chem. C **112**, 17741 (2008).
[27]M. Kratzer, B. C. Bayer, P. R. Kidambi, A. Matković, R. Gajić, A. Cabrero-Vilatela, R. S. Weatherup, S. Hofmann, and C. Teichert, Appl. Phys. Lett. **106**, 103101 (2015).
[28]R. S. Weatherup, B. Eren, Y. Hao, H. Bluhm, and M. B. Salmeron, J. Phys. Chem. Lett. **7**, 1622 (2016).
[29]B. L. Henke, E. M. Gullikson, and J. C. Davis, At. Data Nucl. Data Tables **54**, 181 (1993).
[30]A. C. Ferrari, J. C. Meyer, V. Scardaci, C. Casiraghi, M. Lazzeri, S. Piscanec, K. S. Novoselov, S. Roth, and A. K. Geim, Phys. Rev. Lett. **97**, 187401 (2006).
[31]J. Biener, S. Dasgupta, L. Shao, D. Wang, M. A. Worsley, A. Wittstock, J. R. I. Lee, M. M. Biener, C. A. Orme, S. O. Kucheyev, B. C. Wood, T. M. Willey, A. V. Hamza, J. Weissmüller, H. Hahn, and T. F. Baumann, Adv. Mater. **24**, 5083 (2012).
[32]M. A. Pimenta, G. Dresselhaus, M. S. Dresselhaus, and L. G. Canc, Phys. Chem. Chem. Phys. **9**, 1276 (2007).
[33]G. Ning, Z. Fan, G. Wang, and J. Gao, Chem. Commun. **47**, 5976 (2011).
[34]A. C. Ferrari and J. Robertson, Phys. Rev. B **64**, 75414 (2001).
[35]A. C. Ferrari and J. Robertson, Phys. Rev. B **61**, 14095 (2000).
[36]G. E. Bacon, Acta Cryst. **4**, 558 (1951).
[37]W. S. K. Maier, H. Mehrer, and E. Lessmann, Phys. Status Solidi **78**, 689 (1976).
[38]J. J. Lander, H. E. Kern, and A. L. Beach, J. Appl. Phys. **23**, 1305 (1952).
[39]R. S. Weatherup, C. Baehtz, B. Dlubak, B. C. Bayer, P. R. Kidambi, R. Blume, R. Schloegl, and S. Hofmann, Nano Lett. **13**, 4624 (2013).
[40]R. S. Weatherup, B. C. Bayer, R. Blume, C. Baehtz, P. R. Kidambi, M. Fouquet, C. T. Wirth, R. Schlögl, and S. Hofmann, ChemPhysChem **13**, 2544 (2012).
[41]R. S. Weatherup, L. D. Arsie, A. Cabrero-vilatela, S. Caneva, R. Blume, J. Robertson, R. Schloegl, and S. Hofmann, JACS **137**, 14358 (2015).
[42]L. L. Patera, C. Africh, R. S. Weatherup, R. Blume, S. Bhardwaj, C. Castellarin-cudia, A. Knop-gericke, R. Schloegl, G. Comelli, and S. Hofmann, ACS Nano **7**, 7901 (2013).
[43]A. Cabrero-Vilatela, R. S. Weatherup, P. Braeuninger-Weimer, S. Caneva, and S. Hofmann, Nanoscale **8**, 2149 (2016).
[44]R. S. Weatherup, A. J. Shahani, Z. Wang, K. Mingard, A. J. Pollard, M. Willinger, R. Schloegl, P. W. Voorhees, and S. Hofmann, Nano Lett. **16**, 6196 (2016).
[45]F. Cattaneo, E. Germagnoli, and F. Grasso, Philos. Mag. **7**, 1373 (1962).
[46]A. J. Melmed, J. Appl. Phys. **38**, 1885 (1967).
[47]P. R. Kidambi, C. Ducati, B. Dlubak, D. Gardiner, R. S. Weatherup, M.-B. Martin, P. Seneor, H. Coles, and S. Hofmann, J. Phys. Chem. C **116**, 22492 (2012).
[48]C. T. T. A. Kuper, H. Letaw, L. Slifkin, and E. Sonder, Phys. Rev. **96**, 1224 (1954).
[49]J. Yin, X. Li, J. Zhou, and W. Guo, Nano Lett. **13**, 3232 (2013).
[50]J. G. Alauzun, S. Ungureanu, N. Brun, S. Bernard, P. Miele, R. Backov, and C. Sanchez, J. Mater. Chem. **21**, 14025 (2011).
[51]S. Caneva, R. S. Weatherup, B. C. Bayer, B. Brennan, S. J. Spencer, K. Mingard, A. Cabrero-vilatela, C. Baehtz, A. J. Pollard, and S. Hofmann, Nano Lett. **15**, 1867 (2015).
[52]P. R. Kidambi, R. Blume, J. Kling, J. B. Wagner, C. Baehtz, R. S. Weatherup, R. Schloegl, B. C. Bayer, and S. Hofmann, Chem. Mater. **26**, 6380 (2014).
[53]Y. Gao, Z. Liu, D. Sun, L. Huang, L. Ma, L. Yin, and T. Ma, Nat. Commun. **6**, 8569 (2015).